Published in final edited form as:
Magn Reson Med. 2009 May ; 61(5): 1114–1121. doi:10.1002/mrm.21905.

Spin-Echo Micro-MRI of Trabecular Bone Using Improved 3D FLASE

JF Magland, **MJ Wald**, and **FW Wehrli**
Laboratory for Structural NMR Imaging, Department of Radiology, University of Pennsylvania Medical Center, Philadelphia, Pennsylvania

Abstract

Fast Large-Angle Spin Echo (FLASE) is a common pulse sequence designed for quantitative imaging of trabecular bone micro-architecture. However, imperfections in the nonselective phase-reversal pulse render it prone to stimulated echo artifacts. The problem is further exacerbated at isotropic resolution. Here, a substantially improved RF-spoiled FLASE sequence (sp-FLASE) is described and its performance illustrated with data at 1.5 and 3T. Additional enhancements include navigator echoes for translational motion sensing applied in a slice parallel to the imaging slab. Whereas recent work suggests the use of fully balanced FLASE (b-FLASE) to be advantageous from a SNR point of view, evidence is provided here that the greater robustness of sp-FLASE may outweigh the benefits of minor SNR gain of b-FLASE for the target application of trabecular bone imaging in the distal extremities, sites of exclusively fatty marrow. Results are supported by a theoretical Bloch equation analysis and the pulse sequence dependence of the effective T2 of triglyceride protons. Lastly, sp-FLASE images are shown to provide detailed and reproducible visual depiction of trabecular networks in three dimensions at both anisotropic (137×137×410 μm^3) and isotropic (160×160×160 μm^3) resolutions in the human distal tibia in vivo.

Keywords

FLASE; trabecular bone; micro-MRI

Introduction

Most osteoporotic fractures occur at anatomic sites that contain a significant portion of trabecular bone (TB). Key among these skeletal locations are the vertebrae and the ends of the long bones near the joints where stresses are multi-directional (distal and proximal femur, distal radius and ulna). Even though osteoporosis is always associated with a loss of bone mass, there has been increasing evidence of the role of structure as independent predictors of the mechanical competence of TB (1). This situation has spurred the development of noninvasive imaging techniques for regional quantification of TB architecture (2). MRI has been shown to be particularly useful and both spin-echo and gradient-echo-type pulse sequences are currently in use for this task (3).

Gradient-echo based steady-state free precession (SSFP) techniques, although used widely for TB imaging (4), suffer from signal loss and artifactual broadening of trabeculae due to susceptibility-induced gradient fields at the bone/bone marrow interface (5). The more recently implemented balanced SSFP (b-SSFP) is also sensitive to off-resonance effects (6,7). Although

Contact Information: Jeremy Magland, 1 Founders, University of Pennsylvania Medical Center, 3400 Spruce Street Philadelphia, PA 19104, USA, Voice: 1-215-662-4711, Fax: 1-215-349-5925, Email: Jeremy.Magland@gmail.com

b-SSFP has been shown to produce images with spin-echo type qualities at short repetition times (on the order of 10 ms) (7), this sequence has comparatively low SNR efficiency at the target resolution (~150 μm) due to the necessarily high receiver bandwidth. Indeed, with TR=10 ms, readout time per repetition cannot be much longer than 5 ms (considering the excitation pulse, phase encode, and rewinder gradients), compared with a FLASE readout time of 18 ms per repetition (TR=80ms). These constraints result in an approximate SNR penalty factor of $\sqrt{3}$ for b-SSFP that must be considered when comparing the relative efficiency of the two types of pulse sequences[i]. Of course, some of the signal loss is recovered in b-SSFP by the refocused transverse magnetization carried over from one repetition to the next. However, since the steady-state signal level is heavily T_2-dependent, the relative performance of b-SSFP and FLASE is not straightforward to predict from simulation due to the complex relaxation behavior of fatty marrow protons. In prior work some of the present authors found FLASE to outperform the alternatives in terms of overall image quality and depiction of the trabecular network (8).

In the original formulation of FLASE (5) (hereafter referred to as steady-state FLASE or ss-FLASE), all phase-encoding gradients are rewound, and a consistent spoiler gradient is applied at the end of each repetition. Analogous to SSFP, there are two other variants of this sequence: fully-balanced FLASE (here denoted b-FLASE), and RF-spoiled FLASE (sp-FLASE). In b-FLASE, all gradients are fully rewound at the end of each repetition, so that residual transverse magnetization is utilized in subsequent repetitions. The two steady-state variants (ss-FLASE and b-FLASE) have a higher theoretical SNR efficiency than sp-FLASE, but are prone to ghosting artifacts caused by stimulated echoes resulting from imperfections in the non-selective refocusing pulse. While techniques exist to suppress such artifacts (see for example (9)), it is difficult if not impossible to handle all such ghosting problems, due to the large number of coherence pathways involved (TR=80 is only around one fourth the duration of the principal T_1 component of the lipid resonance in fatty marrow). Furthermore, due to variations in shape and composition of the anatomy and the nature of the spatial B_1 profile, the severity of such artifacts can vary from subject to subject, and even scan to scan, hampering quantitative studies, both cross-sectional and longitudinal. It should be noted that the implementation of b-FLASE (referred to as bSSSE in (10)), organizes the gradients in a manner so as to avoid these ghosting artifacts, at the cost of lost SNR, as will be discussed in detail further below.

Important criteria in the choice of the particular embodiment of the 3D spin-echo pulse sequence (ss-FLASE, b-FLASE, or sp-FLASE) are SNR efficiency and robustness to artifacts. It is therefore essential to accurately predict the relative SNR performance of the three sequences. The SNR gain of b-FLASE over sp-FLASE depends on TR, TE, T_1, and most significantly, T_2 of fatty marrow. In (10), this comparison was made assuming T_2=130 ms (11). However, the difficulty is that the protons in fatty acid triglycerides do *not* have a well-defined T_2 relaxation time that can be assumed for all pulse sequences and the range of sequence parameters. Allerhand (12) first showed that in scalar coupled systems J-coupling leads to variation in the effective T_2 relaxation rate (measured by CPMG) depending on the inter-echo spacing. Henkelman et al (13) more recently showed that the anomalously high signal of fat in fast spin-echo sequences was due to partial suppression of J-modulation dephasing causing inter-echo-time dependent lengthening of the effective T_2.

Several adaptations have previously been made to the original ss-FLASE pulse sequence, including addition of navigator echoes for motion detection (14) and rearrangement of

[i]This effect of readout bandwidth on SNR efficiency is sometimes overlooked in the literature. For example, in (7), the authors state that for b-SSFP, the signal magnitude is largely independent of TR (when TR $\ll$ T2), and therefore the shortest possible TR should be used. However, it is to be noted that when the acquisition time per repetition is constrained by TR, true SNR efficiency does not increase with decreased TR since the bandwidth must be increased proportional to the decrease in TR.

gradients for artifact suppression (9). In this work, we present a substantially enhanced sp-FLASE pulse sequence, disclosed in abstract form in (15). We provide a detailed rationale for the redesigned sequence for imaging of TB architecture at the distal extremities, including an analysis of the theoretical SNR gain of b-FLASE versus sp-FLASE, taking into consideration an appropriate T_2 relaxation time for fatty marrow. We further demonstrate the quality of the depiction of trabecular architecture with images along with 3D bone skeletons for comparison between baseline and six-month follow-up. Finally, we report on the SNR gain achievable at 3 Tesla with the improved pulse sequence, and show how this gain can be used to obtain isotropic (160 μm) resolution images within clinically tolerable scan times as a means to provide what is likely a more accurate representation of trabecular bone network architecture.

Methods

Effective spin-spin relaxation rate

Accurate estimation of T_2 for fatty marrow is essential for the optimal selection of the pulse sequence. Estimation of T_2 is complicated by the multiple chemically shifted components involving homonuclear scalar coupling between protons in fatty acid chains of the triglyceride molecules of which fatty marrow is composed. Therefore, as pointed out earlier, spin-spin relaxation is not a simple mono-exponential process, rather, when measured using a CPMG sequence, for example, the relaxation rate depends on the inter-echo spacing of the refocusing pulses (13). In order to estimate the effective T_2 relaxation time, and hence evaluate the relative SNR performance between b-FLASE and sp-FLASE, a collection of CPMG readouts were acquired on a sample of peanut oil, which, as all edible oils, has chemical make-up close to that of adipose fat. Inter-echo spacing ranged between 4 and 120 ms (in increments of 1 ms), with 8 spin-echo readouts per repetition. A repetition time of 3 seconds was used to ensure sufficient restoration to equilibrium magnetization between acquisitions. An effective T_2 relaxation rate was computed from these measurements as a function of echo number and echo time using the formula:

$$T_{2\text{eff},j}(\text{TE})^{-1} = \frac{-\log \frac{S_j(\text{TE})}{S_j(TE_{j,\min})}}{\text{TE} - TE_{j,\min}}, \quad (1)$$

where $S_j(TE)$ is the magnitude of the signal of the j^{th} echo (j=1….8) at echo time TE, and $TE_{j,min} = 4j$ ms is the minimum acquired echo time. Note that in the case where transverse magnetization decays mono-exponentially, Eq. (1) yields the actual decay rate. The estimated effective T_2 was then used to predict the expected SNR gain of b-FLASE over sp-FLASE according to the formulae of Appendix A.

Pulse sequence

A modification of the FLASE pulse sequence was implemented (Fig. 1). Hereafter, this new sequence is termed *sp-FLASE*, noting that there are further differences between this sequence and the original ss-FLASE besides merely the application of RF-spoiling. The modified sequence incorporates a number of improvements relating to artifact suppression and motion correction.

As in the original sequence, a *non-selective* 180 degree refocusing pulse was used in order to minimize echo time (a selective pulse with sufficiently sharp transition bands would have a prohibitively long duration). As a result, even modest B_1 field inhomogeneity can cause spurious echoes leading to image artifacts. Within a single repetition, this problem is addressed by the use of crusher gradients around the refocusing pulse, as well as phase alternation to push DC artifacts to the edge of the phase-encode field of view (5). A more serious problem occurs

when phase-encoded signal is stored as longitudinal magnetization, reappearing as transverse magnetization in a subsequent repetition. While reorganization of gradients can reduce the severity of such stimulated echoes (9), the relatively short repetition time (TR = 80 ms < T_1 ~ 300 ms) and the presence of two large-flip-angle pulses per repetition create a vast number of coherence pathways (9,16). These types of artifacts are therefore difficult to predict or correct because artifact severity is subject dependent.

To overcome these difficulties, two critical modifications were applied. The dephasing lobe of the readout gradient is placed after (rather than before) the refocusing pulse (at the expense of a small increase in echo time), as suggested in (9). This ensures that any stimulated echo aligns with the main echo in the k_x direction, eliminating the possibility of banding (see Fig. 2). Second, RF-spoiling was implemented by applying a random offset to the large-angle excitation pulse. Such phase randomization ensures that any stimulated echoes are phase-incoherent, preventing systematic artifacts in the reconstructed image.

The sequence also includes improved navigator motion detection. Rather than using residual magnetization after sampling of the imaging signal (14), a separate excitation pulse is used for navigator acquisition. To avoid loss of imaging signal, the navigator pulse excites a slice adjacent to the imaging slab (16). In this manner, navigator signal-to-noise ratio is enhanced, improving overall sensitivity in motion detection. Finally, to reduce the occurrence of aliasing artifacts caused by insufficient field of view in the phase encode direction (Fig. 2), the four corners of k_Y/k_Z space are not acquired, i.e. a cylindrical k-space volume is sampled. The time saved is used to increase the field of view in the in-plane phase-encoding direction. To minimize echo time, the phase-encoding gradients (in the Y direction) were split, with 70% of the moment occurring before, 30% after the refocusing pulse.

Phantom imaging

To demonstrate the sensitivity to ghosting artifacts of b-FLASE, images of a phantom were acquired using both b-FLASE and sp-FLASE. The phantom, designed to mimic the chemical composition and relaxation properties of muscle and yellow bone marrow, consisted of a cylindrical plastic container (approx. 7 cm diameter) filled with agarose gelatin and containing two smaller plastic containers of corn oil (approx. 3 and 4 cm diameter). The size of the oil-filled containers placed within the larger container was chosen to mimic the realtive sizes and locations of the tibia and fibula in the distal ankle. Agarose was doped with GdCl3 and NaCl according to the formula in (17) to reflect the relaxivity and conductivity of knee muscle. Plastic tubes of varying sizes with a wall thickness comparable to that of bone trabeculae were inserted into one of the oil containers.

In vivo imaging

The performance of the pulse sequence is illustrated with data drawn from ongoing clinical research studies at the authors' institution. So far, sp-FLASE has been used in approximately 150 patient examinations on a 1.5 Tesla Siemens Sonata scanner with the following scan parameters: TE = 10.5 ms, TR = 80 ms, flip angle = 140°, readout bandwidth = 32 Hz/pixel, 137×137 μm^2 in-plane resolution, 410 μm slice thickness, and total scan time = 15.5 minutes. The in-plane matrix size was 512×460 for a field-of-view of 70×63 mm^2. A custom-built 2-element surface coil was used. In one pilot study, 30 patients with end-stage renal disease were examined at baseline and again six months later. Half the study subjects were subjected to low-magnitude mechanical stimulation (18). Preliminary data of this study showing a treatment effect on trabecular structural parameters have been reported in abstract form (19) and will be published elsewhere.

The sequence was also implemented at 3 Tesla (Siemens TIM Trio) as part of a reproducibility evaluation in view of a forthcoming drug intervention study. In brief: sp-FLASE images were collected with a custom-built 4-element receive coil array (Insight MRI, Worcester, MA) at the distal tibia. In addition to the standard imaging protocol used at 1.5 Tesla (137×137×410 μm^3 resolution with same parameters as at 1.5T except TE=11.8 ms), images were also acquired at isotropic 160 μm resolution (matrix size 512×400 for a field-of-view of 70×64 mm^2). Since structure analysis requires acquisition of a sufficient volume along z (typically the major loading direction), reduction in slice thickness (by more than a factor of 2) requires at least doubling of the number of slice encodings that, in turn, would double scan time. We have therefore implemented the sequence for parallel imaging along with multi-line, multi-column GRAPPA reconstruction (20) with a kernel size of 3 and 4 points in the readout and phase encode directions, respectively. The calibration region consisted of 60 phase encode lines (out of a total of 400). In this manner, total scan time was maintained at 16 minutes.

The relatively low receiver bandwidth of 32 Hz/pixel was chosen to maximize SNR (the gain from lowering bandwidth must be weighed against the loss from lengthening echo time). Even though the resulting chemical shift effect between fat and muscle is relatively large (approximately 7 pixels or 1 mm at 1.5 Tesla and 14 pixels or 2 mm at 3 Tesla) this is not problematic since the signal-producing tissue of the trabecular bone marrow in the distal extremities is purely fatty, and this region is separated from muscle by the cortex. Further, the signal from fatty acid triglyceride (fat) has a single dominant peak with minor chemically shifted signals of much lower intensity. Lastly, as compared to fat, muscle produces a relatively weak signal for FLASE due to a significantly longer T_1.

SNR Measurement

Comparing signal-to-noise ratios of images acquired with different numbers of receive coils can be more difficult than what one might expect. A typical approach (and the method used here) is to measure the mean signal within the region of interest and divide by the mean signal level in a region of pure noise. However, depending on the method of combining images from separate receive channels, an appropriate adjustment needs to be made. In the present case, channels were combined using a square-root sum-of-squares formula

$$S_j = \sqrt{\sum_{c=1}^{L} \left| S_j^{(c)} \right|^2}, \tag{2}$$

where S_j is the signal of the combined image at the j^{th} pixel, and $S_j^{(c)}$ is the signal for the c^{th} receive channel (L = 2 or 4). In the case of multiple receive coils the measured noise level (mean signal in a region of pure noise) is actually higher than the true noise level within the region of interest. This leads to an artificially low signal-to-noise measurement for four coils as compared to two. To compensate, SNR measurements were adjusted by the following factor:

$$A(L) = \frac{1 \cdot 3 \cdot 5 \cdot \ldots \cdot (2L-1)}{2 \cdot 4 \cdot 6 \cdot \ldots (2L-2)} \sqrt{\frac{\pi}{2}}, \tag{3}$$

as found in (21), where L is the number of coils. Eq. (3) was derived with the assumption that the noise is Gaussian distributed and uncorrelated between channels, and that it has equal standard deviation between channels. Note that in the case of a single receive coil (L=1), this adjustment corresponds to the expression found in (22).

Results and Discussion

The results of the CPMG experiments performed on the peanut oil sample are shown in Fig. 3. It is noted that the overall functional dependence of the effective T_2 is very similar at the two field strengths. Estimated T_2 values are on the order of 60 ms for echo times in the range of 0-200 ms. By Eq. (1), the calculation of the effective T_2 is more reliable for larger values of TE (until of course the noise floor is reached), so the data for TE<20 ms were omitted from the plot. As suggested by the data in Fig. 3, the effective spin-spin relaxation is not a simple mono-exponential process in that the effective T_2 depends on various factors, in particular inter-echo spacing. This functional behavior is contrasted with the flat plot for water. Although effective T_2 for oil increases to over 100 ms for echo times exceeding 600 ms, such values are not relevant for SNR predictions in our situation, where repetition time is 80 ms.

Although the results of the CPMG experiment cannot be used to directly predict the relative SNR performance of the various implementations of FLASE, the data allow selection of an approximate effective T_2 time to be inserted into the signal equations. Note that the echo time for FLASE (around 11 ms) is not the relevant quantity in this analysis, since the signal loss due to echo time is exactly the same between b-FLASE, ss-FLASE, and sp-FLASE. Because the signal gain in b-FLASE and ss-FLASE is caused by magnetization refocused from previous repetitions, the relevant echo times are multiples of TR, i.e. 80 ms, 160 ms, 240 ms, etc. Furthermore, of these echo times, the echo at 80 ms contributes the greatest amount to the signal.

Fig. 4 shows the predicted gain of b-FLASE over sp-FLASE as a function of T_2, at various repetition times. Note that the relatively simple expression for the gain, derived in Appendix A, has no T_1 dependence and interestingly, is equal to the relative gain from balancing in gradient-echo sequences. If T_2=60 ms is used in the formula, as suggested by the CPMG experiments, then the expected gain at TR=80 ms is a mere 3.7%, as compared to a value as high as 19% if a value of 130 ms were chosen for T_2 as in (10). This discrepancy illustrates the importance of selecting an appropriate value of T_2 when estimating the gain. In the present situation (TR=80 ms), the expected gain could be considered insignificant relative to the benefits of spoiling (i.e. artifact reduction).

The plot suggests that decreasing TR to 60 ms would result in a more significant gain from balancing (7.5% for TR=60 ms compared to 3.7% for TR=80 ms). However, there are also significant trade-offs to consider. First, a decrease in TR leaves less time for motion detection navigators and increases the magnitude of inter-repetition spurious encoded longitudinal magnetization. Second, according to Eq. (15), the SNR efficiency (signal at echo time divided by square root of TR) of b-FLASE would decrease by around 6% (assuming TE=12, T1=300 ms, and TR decrease from 80 to 60 ms), virtually eliminating the expected 7.5% gain from balancing in this case.

The images acquired in the phantom experiment, comparing b-FLASE to sp-FLASE, are shown in Fig. 5. The b-FLASE image shows significant ghosting artifacts, resulting from encoded signal stored between repetitions as longitudinal magnetization. It should be noted that such artifacts do not occur in all scans, and can be managed to some extent by arranging crusher gradients appropriately. Further, their presence may be masked by noise at typical SNR values of 10-15 in trabecular bone imaging. However, the vast number of coherence pathways created by the two large-flip-angle pulses greatly complicates the situation, making it virtually impossible to consistently eliminate these subject- (and hardware-) dependent artifacts.

Additional complicating factors arise when scanning at 3D isotropic resolution. For example, crusher gradients (surrounding the refocusing pulse) are only effective if they wind up the magnetization to at least one full cycle within an imaging voxel. At increased resolution (say

160 μm compared to 410 μm slice thickness), this requires significantly longer duration crushers therefore prolonging achievable echo time. A second factor relates to the use of parallel imaging. As mentioned above, one method for dealing with DC artifacts is to push them to the edge of the field of view by alternating the phase of the refocusing pulse (5). However, this technique will fail in the reduction direction of parallel imaging (with R=2) because the artifact will be aliased back into the center of the image. In summary, suppression of stimulated echo artifacts to which b-FLASE is prone, is non-trivial. These difficulties must be weighed against the modest SNR gains expected from balancing.

As mentioned in the introduction, for the implementation of b-FLASE found in (10), termed fully balanced steady-state spin-echo (bSSSE), the gradients are arranged in a manner so as to avoid stimulated echo-induced ghosting artifacts. Specifically, this is achieved by placing the phase-encode gradients in their entirety after the refocusing pulse. However, as compared with the scheme presented here (where 70% phase encoding occurs before the refocusing pulse), this results in increased echo time, and hence lost SNR. In fact, because the refocusing pulse is constrained to occur at time TE/2 after excitation, a lengthening of the post-refocusing phase encode gradients will result in a twofold increase in TE. Therefore, the necessary increase in echo time would be

$$\Delta \mathrm{TE} = 70\% \cdot 2k_{\max}\gamma^{-1}G^{-1}. \quad (4)$$

For example, with gradient amplitude of G=24 mT/m (used in this work) and resolution of 137 μm, the echo time increase would be 5 ms, corresponding to a signal loss (according to Eq. (15)) of 14% (for TR=80 ms and T2=60 ms). Even in the case where G=40 mT/m (a stretch for clinical scanners considering peripheral nerve-stimulation restrictions), echo time would increase by 3 ms, resulting in a predicted signal loss of 9%. In either case, this loss exceeds the expected gain from balancing as predicted above.

Fig. 6 shows pairs of sp-FLASE images of the distal tibia acquired for three of the low-magnitude mechanical stimulation subjects at two time points. The registered cross-sectional images and the 3D cores of the skeletonized images visually highlight the reproducibility achievable with the pulse sequence. Details of the processing procedure are given in (23).

For the anisotropic protocol, the signal-to-noise ratio (obtained in the manner described above, including adjustment by Eq. (3)) derived from five randomly selected images was 18.6±2.4 at 1.5T and 36.8±3.9 at 3T for five randomly selected images at each field strength. The data suggest an approximate twofold increase in SNR by doubling field strength.

In none of the approximately 150 sp-FLASE examinations were there noticeable ghosting or banding artifacts, common with the prior version of ss-FLASE, although some of the images suffered from motion corruption. Because the navigators only detect in-plane translational motion, rotational or through-plane motion cannot be corrected. The authors are currently investigating further techniques that have the potential to correct for these other types of motion, including a recently published version of the autofocusing method (24) which can retrospectively correct for in-plane rotational as well as translational motion. Another possibility is to acquire navigator echoes along more than just two projection directions.

Fig. 7 illustrates the performance achievable at 3T in the isotropic resolution regime (160×160×160 μm^3) in conjunction with parallel imaging (R=2) as described previously. This voxel volume is 53% of 137×137×410 μm^3 (the voxel size of our standard 1.5T clinical protocol). Thus, in order to maintain SNR in the same 16 minutes scan time an increase in intrinsic SNR by a factor of 2 was needed, which was achieved by a combination of increased

field strength (1.5 to 3 Tesla) and more efficient receive coil (recall that a 4-element coil was used at 3T instead of a 2-element coil at 1.5T). Of note in the images of Fig. 7 is the virtual absence of artifacts and the recovery of the plate-like trabecular architecture expected in this young individual, clearly evident in the 3D surface-rendered core.

Conclusion

A new RF-spoiled variant of the basic 3D FLASE pulse sequence, dubbed 'sp-FLASE', for high resolution imaging of trabecular bone, has been introduced. A theoretical T2 analysis suggests that the benefit, in terms of artifact reduction, outweighs the modest SNR loss relative to alternative embodiments such as ss-FLASE and b-FLASE. The robustness of the new protocol is supported by consistent performance over the course of clinical studies involving human subjects.

Appendix

Appendix A

Here we derive a formula for the relative gain in signal-to-noise efficiency of balanced versus spoiled FLASE (i.e. b-FLASE versus sp-FLASE). The spoiled case mirrors the derivation (for the same quantity) found in Chapter 14 of (25). For simplicity we normalize the equilibrium magnetization vector to $(0,0,1)^{\mathrm{T}}$. Let $M_{Y,0}$ and $M_{Z,0}$ be the steady-state transverse and longitudinal magnetization levels immediately before excitation. Immediately after excitation (by a pulse of flip angle φ) we have

$$\begin{aligned} M_{Y,1} &= \cos\varphi \cdot M_{Y,0} + \sin\varphi \cdot M_{Z,0} \\ M_{Z,1} &= -\sin\varphi \cdot M_{Y,0} + \cos\varphi \cdot M_{Z,0}. \end{aligned} \tag{5}$$

Immediately after the refocusing pulse (occurring at half the echo time), we have

$$\begin{aligned} M_{Y,2} &= \cos\varphi \cdot e^{-\mathrm{TE}/2T_2} \cdot M_{Y,0} + \sin\varphi \cdot e^{-\mathrm{TE}/2T_2} \cdot M_{Z,0} \\ M_{Z,2} &= -1 + e^{-\mathrm{TE}/2T_1} + \sin\varphi \cdot e^{\mathrm{TE}/2T_1} \cdot M_{Y,0} - \cos\varphi \cdot e^{-\mathrm{TE}/2T_1} \cdot M_{Z,0}, \end{aligned} \tag{6}$$

and at the end of the repetition period:

$$\begin{aligned} M_{Y,3} &= \cos\varphi \cdot e^{-\mathrm{TR}/T_2} \cdot M_{Y,0} + \sin\varphi \cdot e^{-\mathrm{TR}/T_2} \cdot M_{Z,0} \\ M_{Z,3} &= 1 - 2e^{-(\mathrm{TR}-\mathrm{TE}/2)/T_1} + e^{-\mathrm{TR}/T_1} + \sin\varphi \cdot e_1{}^{-\mathrm{TR}/T_1} \cdot M_{Y,0} - \cos\varphi \cdot e_1{}^{-\mathrm{TR}/T_1} \cdot M_{Z,0}. \end{aligned} \tag{7}$$

In the case of sp-FLASE, we assume the initial transverse magnetization is zero ($M_{Y,0}=0$), and upon setting $M_{Z,3}=M_{Z,0}$, we obtain:

$$M_{Z,0} = \frac{1 - 2e^{-(\mathrm{TR}-\mathrm{TE}/2)/T_1} + e^{-\mathrm{TR}/T_1}}{1 + \cos\varphi \cdot e_1{}^{-\mathrm{TR}/T_1}}, \tag{8}$$

yielding a signal strength at echo time of

$$\tilde{S}_{\mathrm{spoiled}} = \frac{1 - 2e^{-(\mathrm{TR}-\mathrm{TE}/2)/T_1} + e^{-\mathrm{TR}/T_1}}{1 + \cos\varphi \cdot e^{-\mathrm{TR}/T_1}} \cdot \sin\varphi \cdot e^{-\mathrm{TE}/T_2}. \tag{9}$$

This expression is maximized by setting $\cos\varphi = -e^{-\mathrm{TR}/T_1}$ to yield an optimized signal of

$$S_{\text{spoiled}} = \frac{1 - 2e^{-(\mathrm{TR}-\mathrm{TE}/2)/T_1} + e^{-\mathrm{TR}/T_1}}{\sqrt{1 - e^{-2\mathrm{TR}/T_1}}} \cdot e^{-\mathrm{TE}/T_2}. \tag{10}$$

For b-FLASE, the transverse magnetization carries over, and we set $M_{Y,3}=M_{Y,0}$ and $M_{Z,3}=M_{Z,0}$ to obtain the following matrix equation:

$$\begin{bmatrix} 1-\cos\varphi\cdot e^{-\mathrm{TR}/T_2} & -\sin\varphi\cdot e^{-\mathrm{TR}/T_2} \\ -\sin\varphi\cdot e^{-\mathrm{TR}/T_1} & 1+\cos\varphi\cdot e^{-\mathrm{TR}/T_1} \end{bmatrix} \begin{bmatrix} M_{Y,0} \\ M_{Z,0} \end{bmatrix} = \begin{bmatrix} 0 \\ 1-2e^{-(\mathrm{TR}-\mathrm{TE}/2)/T_1}+e^{-\mathrm{TR}/T_1} \end{bmatrix}. \tag{11}$$

Solving this system gives:

$$\begin{bmatrix} M_{Y,0} \\ M_{Z,0} \end{bmatrix} = \frac{1-2e^{-(\mathrm{TR}-\mathrm{TE}/2)/T_1}+e^{-\mathrm{TR}/T_1}}{1-e^{-\mathrm{TR}/T_1}e^{-\mathrm{TR}/T_2}+\cos\varphi(e^{-\mathrm{TR}/T_1}-e^{-\mathrm{TR}/T_2})} \begin{bmatrix} \sin\varphi\cdot e^{-\mathrm{TR}/T_2} \\ 1-\cos\varphi\cdot e^{-\mathrm{TR}/T_2} \end{bmatrix}, \tag{12}$$

and a signal at echo time of:

$$S_{\text{balanced}} = \frac{1-2e^{-(\mathrm{TR}-\mathrm{TE}/2)/T_1}+e^{-\mathrm{TR}/T_1}}{1-e^{-\mathrm{TR}/T_1}e^{-\mathrm{TR}/T_2}+\cos\varphi(e^{-\mathrm{TR}/T_1}-e^{-\mathrm{TR}/T_2})} \cdot \sin\varphi\cdot e^{-\mathrm{TE}/T_2}. \tag{13}$$

The optimal flip angle is obtained by setting

$$\cos\varphi = \frac{-(e^{-TR/T_1}-e^{-TR/T_2})}{1-e^{-TR/T_1}e^{-TR/T_2}}, \tag{14}$$

for the following optimal signal:

$$S_{\text{balanced}} = \frac{1-2e^{-(TR-TE/2)/T_1}+e^{-TR/T_1}}{\sqrt{(1-e^{-2TR/T_1})(1-e^{-2TR/T_2})}} \cdot e^{-TE/T_2}. \tag{15}$$

Comparing (7) with (12), we therefore see that switch from spoiled to balanced FLASE results in a signal gain of

$$\mathrm{SNR}_{\text{gain}} = \left(1-e^{-2TR/T_2}\right)^{-1/2}. \tag{16}$$

Note that this expression depends only on TR/T_2 (and not on TE and T_1), and that this is precisely the same gain factor obtained from switching between spoiled and balanced gradient echo (see (25)).

Acknowledgement

This research was supported by NIH grants RO1 AR41443, RO1 AR53156 and K25 EB007646. The authors are indebted to Catherine Jones for acquiring the images in Fig. 6.

References

1. Seeman E, Delmas PD. Bone quality–the material and structural basis of bone strength and fragility. N Engl J Med 2006;354(21):2250–2261. [PubMed: 16723616]
2. Genant HK, Jiang Y. Advanced imaging assessment of bone quality. Ann N Y Acad Sci 2006;1068:410–428. [PubMed: 16831940]
3. Wehrli FW. Structural and functional assessment of trabecular and cortical bone by micro magnetic resonance imaging. J Magn Reson Imaging 2007;(2):390–409. [PubMed: 17260403]
4. Majumdar S. Magnetic resonance imaging of trabecular bone structure. Top Magn Reson Imaging 2002;13(5):323–334. [PubMed: 12464745]
5. Ma J, Wehrli FW, Song HK. Fast 3D large-angle spin-echo imaging (3D FLASE). Magnetic Resonance in Medicine 1996;35:903–910. [PubMed: 8744019]
6. Scheffler K, Lehnhardt S. Principles and applications of balanced SSFP techniques. Eur Radiol 2003;13 (11):2409–2418. [PubMed: 12928954]
7. Banerjee S, Han ET, Krug R, Newitt DC, Majumdar S. Application of refocused steady-state free-precession methods at 1.5 and 3 T to in vivo high-resolution MRI of trabecular bone: simulations and experiments. J Magn Reson Imaging 2005;21(6):818–825. [PubMed: 15906346]
8. Techawiboonwong A, Song H, Saha P, Wehrli F. Implications of pulse sequence in structural imaging of trabecular bone. J Magn Reson Imaging 2005;22:647–655. [PubMed: 16215967]
9. Vasilic B, Song H, Wehrli F. Coherence induced artifacts in large-flip-angle steady-state spin-echo imaging. Magnetic Resonance in Medicine 2004;52:346–353. [PubMed: 15282817]
10. Krug R, Han ET, Banerjee S, Majumdar S. Fully balanced steady-state 3D-spin-echo (bSSSE) imaging at 3 Tesla. Magn Reson Med 2006;56(5):1033–1040. [PubMed: 16986110]
11. Gold GE, Han E, Stainsby J, Wright G, Brittain J, Beaulieu C. Musculoskeletal MRI at 3.0 T: relaxation times and image contrast. AJR Am J Roentgenol 2004;183(2):343–351. [PubMed: 15269023]
12. Allerhand A, Gutowsky HS, Jonas J, Meinzer RA. Nuclear magnetic resonance methods for determining chemical-exchange rates. J Am Chem Soc 1966;88(14):3185–3193. [PubMed: 5946590]
13. Henkelman RM, Hardy PA, Bishop JE, Poon CS, Plewes DB. Why fat is bright in RARE and fast spin-echo imaging. J Magn Reson Imaging 1992;2(5):533–540. [PubMed: 1392246]
14. Song HK, Wehrli FW. In vivo micro-imaging using alternating navigator echoes with applications to cancellous bone structural analysis. Magnetic Resonance in Medicine 1999;41:947–953. [PubMed: 10332878]
15. Magland, J.; Jones, C.; Wald, M.; Wehrli, FW. Spin-Echo Micro-MRI of Trabecular Bone Using an Improved 3D FLASE Sequence. Berlin, Germany: ISMRM; 2007. p. 382
16. Magland J, Vasilic B, Wehrli FW. Fast low-angle dual spin-echo (FLADE): a new robust pulse sequence for structural imaging of trabecular bone. Magn Res Medicine 2006;55(3):465–471.
17. Kato H, Kuroda M, Yoshimura K, Yoshida A, Hanamoto K, Kawasaki S, Shibuya K, Kanazawa S. Composition of MRI phantom equivalent to human tissues. Med Phys 2005;32(10):3199–3208. [PubMed: 16279073]
18. Rubin C, Recker R, Cullen D, Ryaby J, McCabe J, McLeod K. Prevention of postmenopausal bone loss by a low-magnitude, high-frequency mechanical stimuli: a clinical trial assessing compliance, efficacy, and safety. J Bone Miner Res 2004;19(3):343–351. [PubMed: 15040821]
19. Jones, CE.; Wehrli, FW.; Magland, JF.; Rubin, CT.; NIhtianova, SA.; Leonard, MB. Structural Implications of low-magnitude mechanical stimulation in a pilot study of patients with renal osteodystrophy evaluated with the MRI-based Virtual Bone Biopsy. Honolulu, HI: ASBMR; 2007. p. S133
20. Wang Z, Wang J, Detre JA. Improved data reconstruction method for GRAPPA. Magn Reson Med 2005;54(3):738–742. [PubMed: 16088880]
21. Constantinides CD, Atalar E, McVeigh ER. Signal-to-noise measurements in magnitude images from NMR phased arrays. Magn Reson Med 1997;38(5):852–857. [PubMed: 9358462]
22. Henkelman RM. Measurement of signal intensities in the presence of noise in MR images. Med Phys 1985;12(2):232–233. [PubMed: 4000083]

23. Magland J, Wehrli FW. Trabecular Bone Structure Analysis in the Limited Spatial Resolution Regime of In Vivo MRI. Acad Radiol. 2008

24. Lin W, Ladinsky GA, Wehrli F, Song HK. Image metric-based correction (autofocusing) of motion artifacts in high-resolution trabecular bone imaging. J Magn Reson Imaging 2007;26:191–197. [PubMed: 17659555]

25. Bernstein, MA.; King, KF.; Zhou, XJ. Handbook of MRI Pulse Sequences. Burlington, MA: Elsevier Academic Press; 2004.

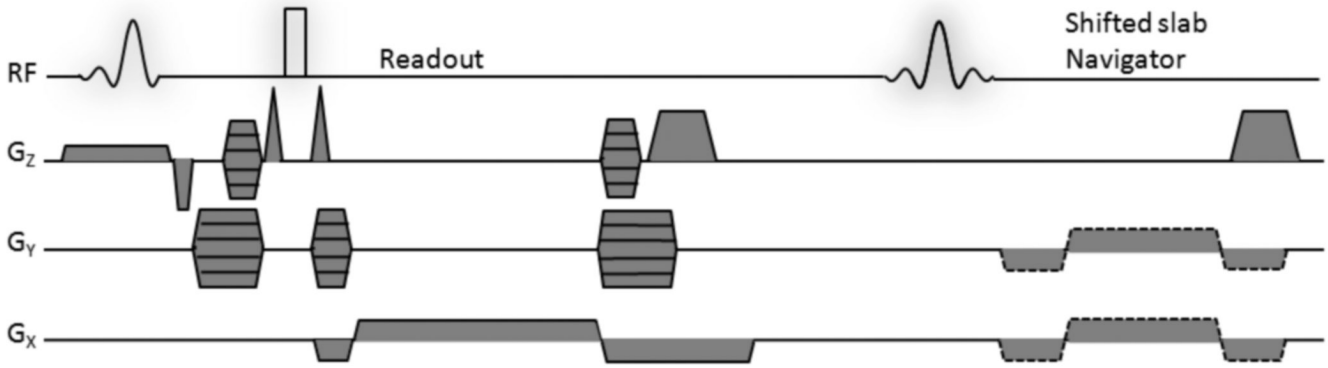

Fig. 1.

Pulse sequence diagram of sp-FLASE. Modifications include placement of the prephasing lobe of the readout gradient after the refocusing pulse, applying RF-spoiling to the imaging excitation pulse, and incorporation of a separate out-of-slab navigator excitation pulse for motion detection. The structure of b-FLASE is essentially the same as in sp-FLASE except that it does not have spoiler gradients along Z and does not employ RF-spoiling.

Fig. 2.
Illustration of banding and aliasing artifacts in a 3D ss-FLASE scan acquired prior to the time that the present modifications were implemented.

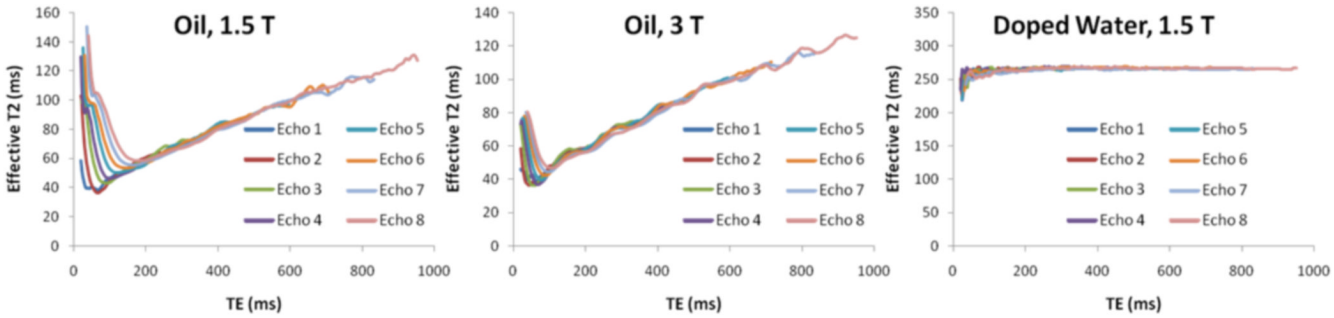

Fig. 3.

Effective T_2 as a function of TE for varying CPMG echo number in homogeneous oil at 1.5 Tesla (left) and 3.0 Tesla (center), and doped water (control) at 1.5 Tesla (right).

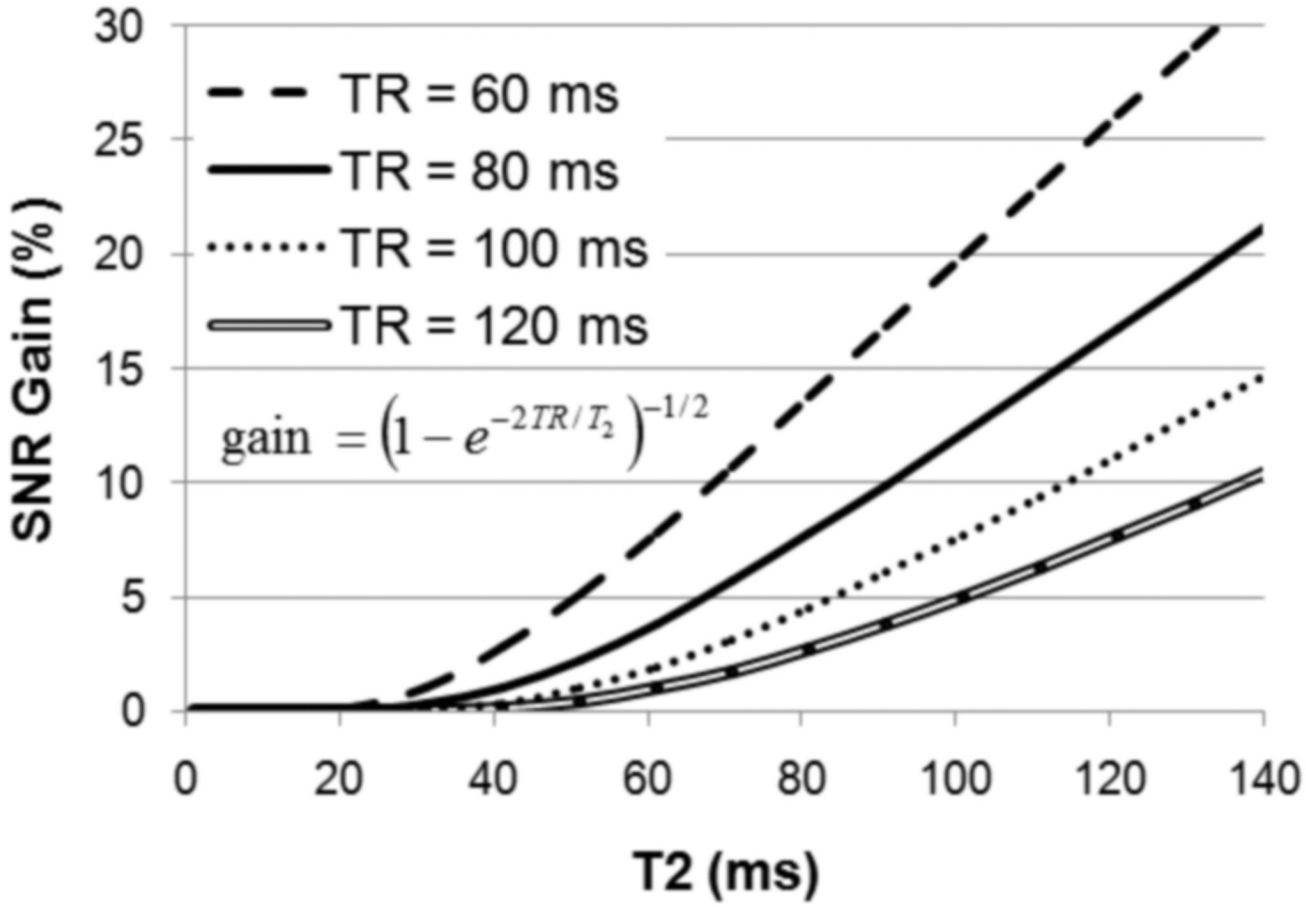

Fig. 4.

Theoretical SNR gain of b-FLASE over sp-FLASE as a function T_2 for various repetition times, equal to the ratio of Eqs. (15) and (10). For T_2 = 60 ms, and TR = 80 ms, the gain is less than 5%.

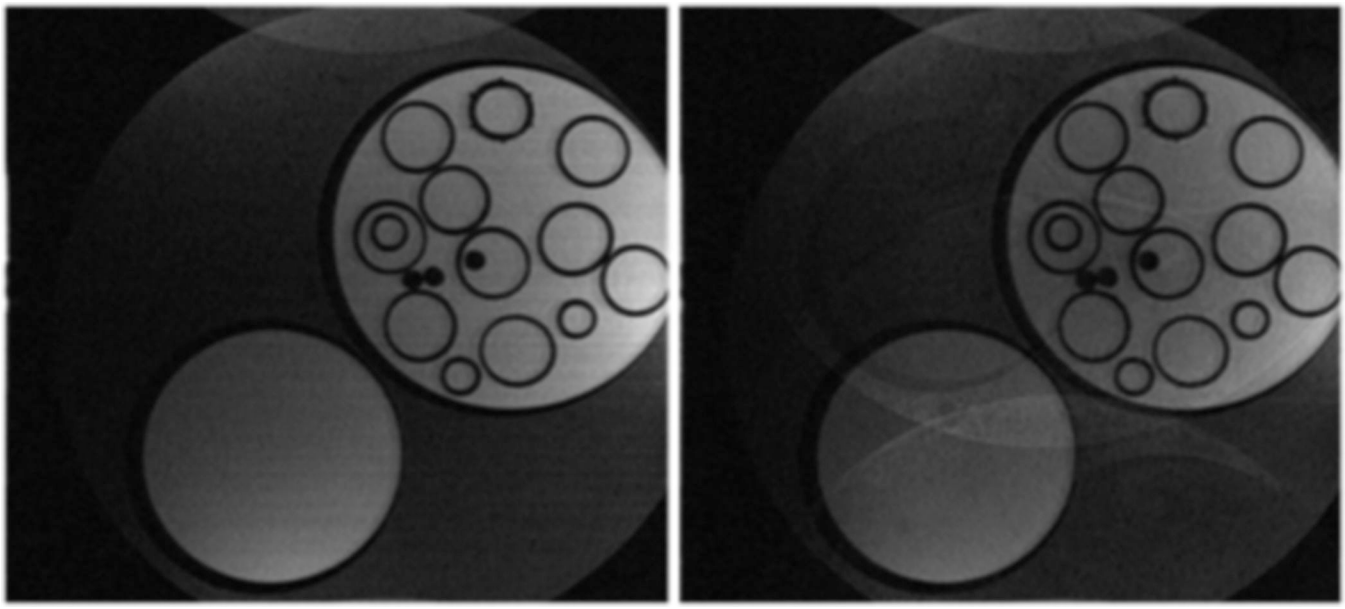

Fig. 5.
Images of oil/agarose phantom using sp-FLASE (left) and b-FLASE (right). The image for the balanced sequence shows a ghosting artifact resulting from spurious echoes. These echoes also occur in sp-FLASE, but are phase-incoherent throughout k-space, and therefore do not cause an observable image artifact.

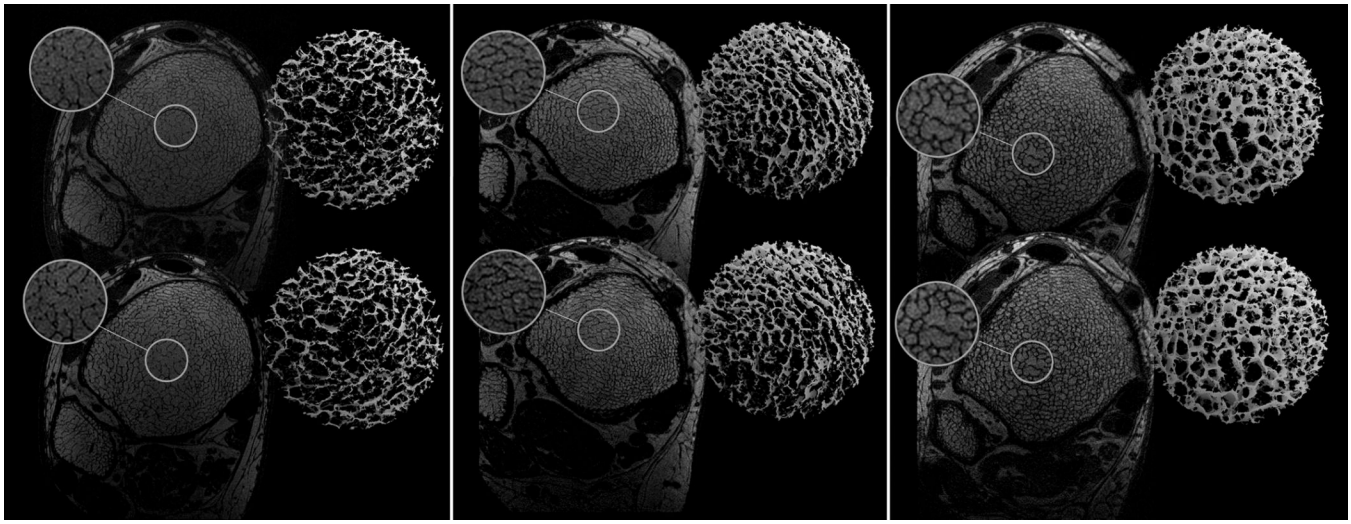

Fig. 6.
Baseline (top) and 6-month follow-up (bottom) sp-FLASE images of the distal tibia acquired from three subjects who were part of an intervention study in which subjects with renal osteodystrophy were evaluated at two time points: a) female, 45 yrs; b) female, 35 yrs; c) male, 61 yrs. Magnifications and 3D skeleton cores show visually reproducible depiction of trabecular architecture.

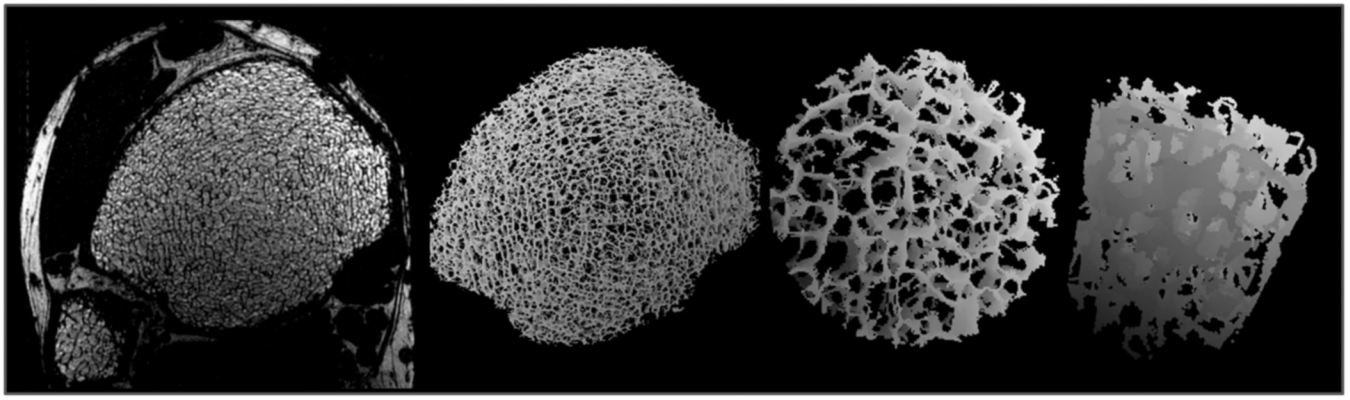

Fig. 7.
3D sp-FLASE images of the distal tibial metaphysis in a 31 year old male subject. Images were acquired at 3 Tesla at isotropic resolution of 160μm with parallel imaging using a 4-element surface-coil array in 16 minutes scan time: a) one of 60 slices; b) surface-rendered skeleton map of trabecular region; c) magnified cylindrical subvolume extracted from b); d) cutaway of c) rotated to show a longitudinal view. For details see text.